Science of the Total Environment 705 (2020) 135773

Contents lists available at ScienceDirect

Science of the Total Environment

journal homepage: www.elsevier.com/locate/scitotenv

The effects of hydrodynamics on the three-dimensional downstream migratory movement of Atlantic salmon

Ana T. Silva [a,*], Kim M. Bærum [b], Richard D. Hedger [a], Henrik Baktoft [c], Hans-Petter Fjeldstad [d], Karl Ø. Gjelland [e], Finn Økland [a], Torbjørn Forseth [a]

[a] Norwegian Institute for Nature Research, P.O. Box 5685 Torgarden, 7485 Trondheim, Norway
[b] Norwegian Institute for Nature Research, Fram Centre, Lillehammer, Fakkelgården, 2624 Lillehammer, Norway
[c] National Institute of Aquatic Resources, Section for Freshwater Fisheries and Ecology, Technical University of Denmark, Vejlsøvej 39, 8600 Silkeborg, Denmark
[d] SINTEF Energy, Sem Sælands vei 11, 7034 Trondheim, Norway
[e] Norwegian Institute for Nature Research, Fram Centre, PO Box 6606, Langnes, 9296 Tromsø, Norway

HIGHLIGHTS

- Development of a combined 3D hydraulic- individual fish -based behavioural model.
- 3D movement of salmon smolts partly results from adjustment of fish to flow motion.
- Fish can diverge from flow direction at speeds higher than their prolonged speed.
- Scientific foundation for improving engineering solutions for safe fish migration.

GRAPHICAL ABSTRACT

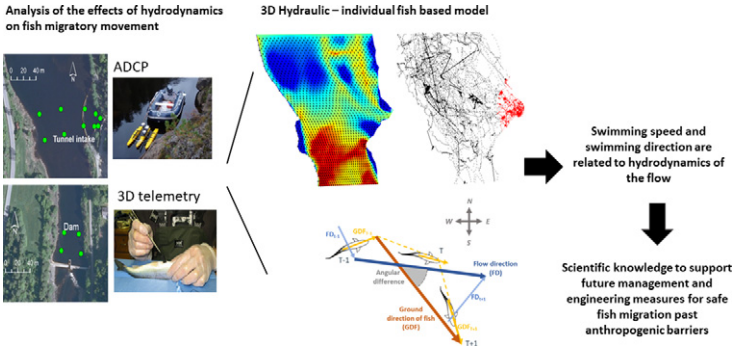

ARTICLE INFO

Article history:
Received 8 October 2019
Received in revised form 19 November 2019
Accepted 24 November 2019
Available online 27 November 2019

Editor: Jay Gan

Keywords:
2D and 3D-telemetry
Downstream migration
Atlantic salmon smolts
Fish migration
Fish behaviour
Hydraulics

Data availability
Data available upon request

ABSTRACT

Anthropogenic structures in rivers are major threats for fish migration and effective mitigation is imperative given the worldwide expansion of such structures. Fish behaviour is strongly influenced by hydrodynamics, but little is known on the relation between hydraulics and fish fine scale-movement. We combined 3D Computational fluid dynamics modelling (CFD) with 2D and 3D fish positioning to investigate the relation between hydrodynamics and the downstream movement of Atlantic salmon smolts (*Salmo salar*). We show that fish use fine-scale flow velocity and turbulence as navigation cues of fine-scale movement behaviour. Tri-dimensional swimming speed and swimming direction can be explained by adjustments of fish to flow motion, which are linked to fish swimming mode. Fish diverge from the flow by swimming at speeds within or higher than their prolonged speeds (0.38–0.73 m s^{-1}). Flow direction plays a pivotal role on fish swimming performance, with high upstream and downwards velocities impacting swimming the most. Turbulence is also influential, by benefiting swimming performance at low TKE (< 0.03 m^2 s^{-2}) or constraining it at higher levels. We show that fish behaviour is affected by interactions of several hydraulic variables that should be considered jointly.

* Corresponding author at: Norwegian Institute for Nature Research - NINA, P.O. Box 5685 Torgarden, 7485 Trondheim, Norway
E-mail address: ana.silva@nina.com (A.T. Silva).

https://doi.org/10.1016/j.scitotenv.2019.135773

1. Introduction

During life fish may travel considerable distances for different purposes (Lucas and Baras 2001; Brönmark et al. 2013). Migratory movement is a fundamental characteristic of fishes, with strong impacts on their ecology and population size (Hugh Dingle and Drake 2007). Migratory movements in rivers are often blocked or obstructed by the presence of anthropogenic structures such as dams, weirs or water abstraction facilities (Lucas and Baras 2001; Poff et al. 1997; Silva et al. 2018) and mitigating fish migration barriers remain a major challenge worldwide with over half of the world's major rivers fragmented by >50,000 large dams (Nilsson et al. 2005). Mitigation efforts are hampered by the poor knowledge on the migratory movements and the fine-scale choice of migration trajectory of fish, particularly in complex hydrodynamic river systems. A functional understanding of fish migration in river systems could strongly aid the development of efficient guiding or bypass structures (Goodwin et al. 2014).

Spatial and temporal migratory movement results from a complex decision process ultimately linked to fitness costs and benefits of different swimming strategies (Chapman et al. 2011). Swimming performance in rivers is a behavioural response expected to be strongly affected by fluid motion (Goodwin et al. 2014) but also by a suite of other *endo*- and exogenous factors (Cotel et al., 2006; Lupandin 2005). Heterogeneity of flows in riverine systems may be perceived by fish through their hydrodynamic sensory system (lateral line, Bleckmann and Zelick 2009) and used as cues driving fish behavioural responses (Coutant 2001; Montgomery et al., 1997; Silva et al. 2011; Voigt et al. 2000). The functional components of the lateral line (the superficial neuromast and the canal neuromast) allow fish to discriminate both frequency and amplitude of a constant frequency wave stimulus as well as abrupt frequency changes from the mean flow (Bleckmann and Zelick 2009). Fish can thus determine flow direction and flow velocity that inform on both water velocity and turbulence, that can be used as source of information for navigation (Bleckmann and Zelick 2009). The sensory system enables fish to explore and identify favourable flow conditions for propulsion, leading to different optimal orientation and direction-of-motion responses adopted by fish during their journey. How fish use hydrodynamic cues to guide fine-scale swim trajectory selection during migration is still poorly understood and has been mainly explored in laboratory conditions. However, Goodwin et al. (2014) recently combined computational fluid dynamics (CFD) modelling and a behavioural model to reproduce juvenile Pacific salmonids movements across a range of flow field conditions in the Columbia/Snake River system, clearly illustrating the value of such knowledge for management and engineering design. Nevertheless, this work lacked on providing detailed information on the link between fine-scale fish behaviour and hydraulics. Here we provide such data by exploring and analysing the effects of hydrodynamics on fish three-dimensional fine-scale movement (swimming speed and fish swimming direction) and migratory trajectory of Atlantic salmon (*Salmo salar*) smolts.

We combined high-resolution 3D computational fluid dynamics (CFD) modelling with high-resolution 2D and 3D acoustic telemetry under different hydraulic conditions in the vicinity of an intake to a hydropower plant. By doing so we also explored the established hypothesis that migrating Atlantic salmon smolts follow the main flow during downstream migration (Rivinoja 2005; Williams et al., 2012). Results were linked to the different swimming capacity modes (sustained, prolonged and burst) of salmon smolt (Booth et al. 1997).

2. Material and methods

2.1. Study site

This study was conducted in one of the largest salmon-bearing rivers in southern Norway, the River Mandalselva (58° N, 7° E). This river has a high annual production of smolts (≈ 54,000–120,000 smolts a^{-1}; see Ugedal et al. 2006). However, this river is also characterised by the presence of six hydropower plants (see Fjeldstad et al. 2012 for details) which affect smolt production due to flow regime-induced changes in discharge and wetted area and turbine mortality resulting from downstream-migrating smolts entering turbine intakes. This study focused on the watercourse around the intake to the Laudal hydropower plant (HPP) during May 2015 (the smolt migratory period in this river), located midway in salmon producing part of the river. The intake area of this HPP (7.6 m × 13.9 m, width x depth) is composed of a vertical wall reaching to 2 m depth and extending the full width of the intake area and of a vertical bar rack below this wall (13 m width, 70°angle, 80 mm vertical bar spacing) extending to the bottom of the water column. To cope with the high flows resulting from precipitation and snow melt that commonly occur during the smolt migratory season, the Laudal HPP facility normally uses its full capacity (110 $m^3 s^{-1}$) in combination with flood spill over a small concrete weir (50 m × 2.5 m, width x height) located 500 m downstream of the intake (Fig. 1). This structure comprises a lateral sluice gate (3 × 1 m) with a full flow capacity of approximately 20 $m^3 s^{-1}$ and a pool and weir fishway in the middle part of it.

2.2. Biological data collection

The downstream movement of Atlantic salmon smolts in the vicinity of the intake of the Laudal HPP was analysed to assess the effect of hydrodynamics on fish migration movements. Ninety-two smolts were caught using a floating rotary screw trap at Hesså 7 km upstream of the intake (see Fjeldstad et al. 2012 for details). Fish were anaesthetized by immersion in a 0.7 mL L solution of 2-phenoxy-ethanol (EC No 204–589-7; Sigma Chemical Co., St. Louis, MO, USA), and weighed (W) and measured (total length L_t) from which Fulton Conditioner Factor (K) was derived. Each smolt was then surgically tagged with an acoustic tag (Lotek M-626, burst interval 5 s, signal definition file 1.1.1) implanted in the peritoneal cavity. All handling and tagging were conducted according to the Norwegian regulations for treatment and welfare of animals (permit ID 7636). Fourteen hydrophones (Lotek 200 kHz WHS 3050, Lotek Wireless Inc., Newmarket, Ontario, Canada) were positioned in the main water course and intake area of the Laudal hydropower weir (Fig. S1) (distance to surface 0.7 m–3.1 m). In the intake area where the water depth was higher (max 13 m), the hydrophones were mounted in a 3D array (four near the surface and four near the bottom) allowing for estimation of fish position in the vertical dimension. Smolt trajectories were estimated using YAPS (Yet Another Positioning Solver; Baktoft et al., 2017). YAPS estimates the transmitter position for each transmission (i.e. with 5 s interval in this study) and provides error estimates of each estimated position. After post-processing the data, the positions of 76 smolts (mean L_t: 14.70 ± 1.05 SD cm; mean W: 23.93 ± 5.91 SD g) were analysed. Positions with an error estimate larger than 5 m were excluded from analyses. In total 21,607 positions were used for the analysis.

2.3. Hydrodynamics data collection and modelling

Bathymetry and depth integrated horizontal water velocities were measured bank-to-back criss-cross transects from 150 m upstream of the hydropower plant intake to 300 m downstream using a RiverSurveyor S9 (Sontek) Acoustic Doppler Current Profiler (ADCP). Hydrodynamics were then simulated by the 3-dimensional CFD model SSIIM (Sediment Simulation In Intakes with Multiblock option; Olsen 2009) through the discretization of the flow using a grid of 300 × 300 dimensionally finite hexahedral cells (median length = 0.5 m) in the horizontal domain, and 10 cells in the vertical domain. This grid was used to study the flow in the main section of the river (main water course). For a higher resolution characterization of the hydrodynamics in front of the intake area, a second grid was developed with a finer mesh of 100 × 100 finite hexahedral cells in the horizontal domain

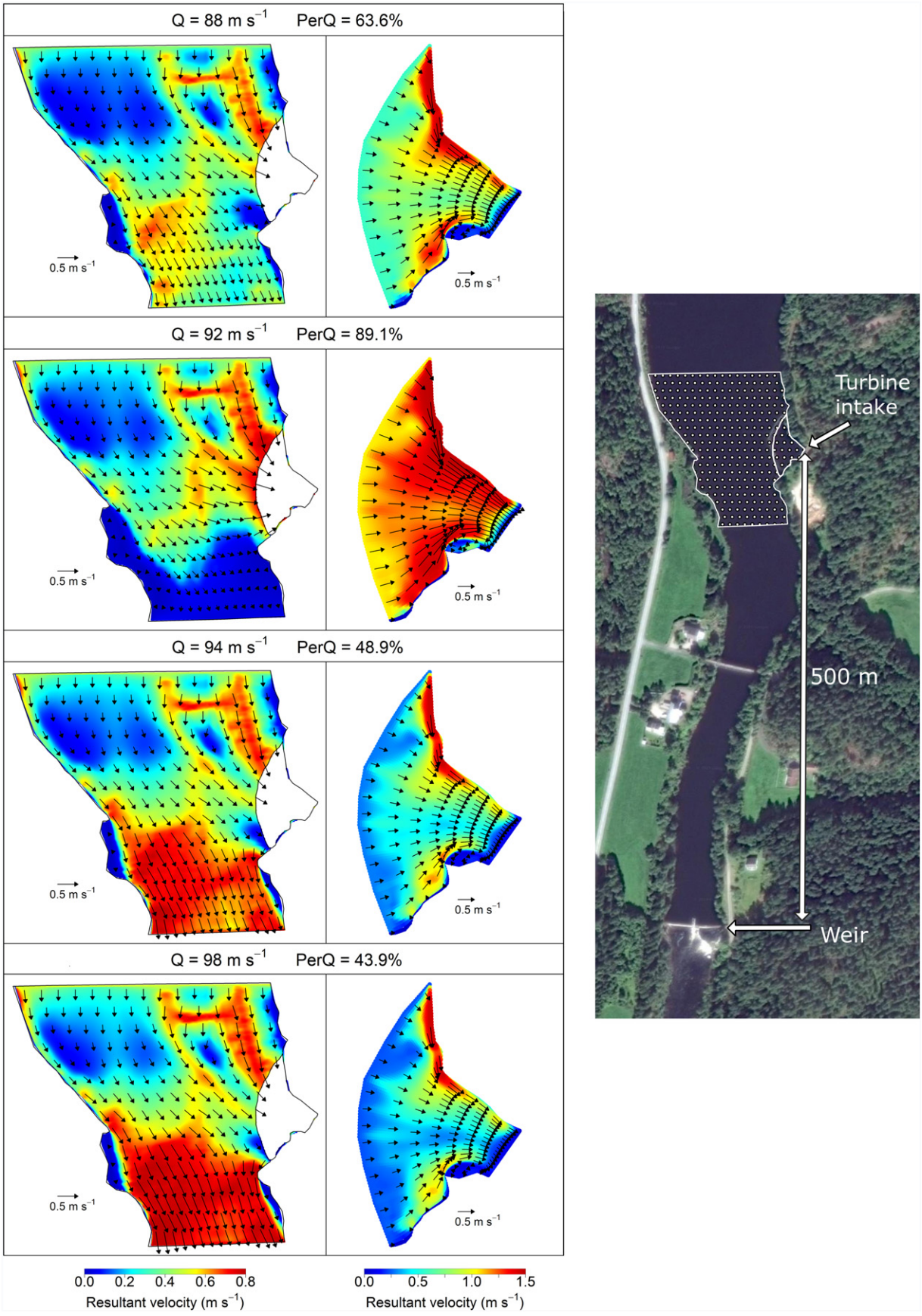

Fig. 1. Predicted resultant velocity in main water course (left panels) and intake area (right panel) at Z = 0.5 m from the surface. A satellite image showing the location of the turbine intake, weir and study area is also included.

(median horizontal side length = 0.08 m) and 10 cells in the vertical domain. Boundary conditions based on bathymetry data were assigned, a fixed flow rate and water elevation were allocated to the entrance and exit of the system and the remaining boundaries were assumed to be impermeable solid banks. Simulations were run for a range of discharges (Q = 82, 92, 94 and 98 $m^3\ s^{-1}$) and corresponding percentage flows into the bypass (PerQ = 64%, 89%, 49%, 44%) representative for the flow conditions experienced by smolts when migrating through the system. Three-dimensional components of velocity (longitudinal: u^+ upstream, u^- downstream; transversal: v^+ right to left bank, v^- left to right bank; vertical: w^+ upwards, w^- downwards), turbulent kinetic energy (TKE), and the rate of turbulence dissipation, epsilon (ε) were obtained for each cell by solving the Navier-Stokes equation for turbulent flow, with the k-ε turbulence model being discretized with a control-volume approach (for details see Olsen 2009). Turbulent flows are not reproducible but the statistical properties such as space and time average, correlations functions over large samples are predictable. Averaging processes decompose the instantaneous flow quantity into a mean and fluctuating component and the temporal average can then be used to describe turbulent flow, as done in the present study. The resultant velocities for horizontal (V_{uv}), longitudinal vertical planes (V_{uw}) (Fig. 1) and the total resultant velocity (V_r) were also calculated for each cell. Model predictions were validated using the ADCP measurements by comparing simulated and observed horizontal flow directions (circular correlation test using the cor.circular function of the circular-library in R Core Team, 2017) and horizontal resultant flow velocities (Pearson's correlation test using the cor.test function of the stats-library).

2.4. Combining fish movement and hydrodynamics

To analyse the impact of hydraulics on the migratory movement of smolts through the domain, the hydraulic properties of each Cartesian position of the individual smolt (obtained by the telemetry system) were assigned from those corresponding to the nearest hexahedral cell reference node in the hydraulic model. Data on the individual positions were then analysed in combination with the hydraulic properties generated by the CFD model for each cell. In the main water course only, the hydraulic data generated at approximately 50 cm from the surface was used as we assumed that smolts migrate in near-surface waters (Thorstad et al. 2012).

Fish behaviour was analysed with regard to angular difference and swimming speed. Angular difference was defined as the absolute difference between ground direction of the fish and the flow direction (in degrees), and indicates the swimming direction of the fish relative to the flow direction. This differs from the concept of fish swimming orientation, which involves knowledge on the orientation of the body of the fish.

Swimming speed was calculated as follows:

$$S_r = \sqrt{S_x^2 + S_y^2 + S_z^2} \quad (1)$$

where S_x, S_y and S_z are swimming speeds in x, y and z directions, respectively. S_x, S_y and S_z were calculated as follows.

$$S_x = G_x - u;\ S_y = G_y - v;\ S_z = G_z - w \quad (2)$$

where G_x, G_y and G_z are the ground speeds of the fish in x, y and z dimensions and u, v and w are the water velocity components in the same dimensions. Ground speeds and swimming speed of fish in time (t) were calculated as displacement from time t-1 to time t + 1. These were analysed with respect to hydraulic properties calculated in time (t) using the Finite Differential method (the central difference; Chen 2006). The Finite Differential method is a discretization method that allows the generation of trajectories with continuous potential models, by dividing the total integration in several smalls steps of fixed time period (σt). The total interaction on each particle at time (t) is then the sum of interactions from other particles. In this method the force is assumed to be constant during the time step (t) and (t + σt). Forces of particles in new positions can then be determined.

Fish maximum sustained, prolonged and burst swimming speeds were estimated based on Booth et al. (1997) using the average body length (Bl. s^{-1}) of the fish and ambient temperature: sustained swimming speed = 2.6 Bl. $s^{-1} \approx 0.38$ m s^{-1}; prolonged swimming speed = 2.5–4.5 Bl. $s^{-1} \approx 0.37$–0.66 m s^{-1}, average 0.5 m s^{-1}; and burst swimming speed = 5 Bl. $s^{-1} \approx 0.73$ m s^{-1}. These were analysed alongside with the resultant flow velocities to identify the swimming modes that fish used when swimming under different hydraulic conditions.

2.5. Statistical analysis

The influence of flow properties (Q and PerQ), smolt characteristics (W and K) and location of first detection (either right bank, central right, central left or left bank) on smolt final destination (either migrating downstream or entering the turbine intake) was determined using generalized linear modelling (binomial error distribution) using the glm function of the stats-library. This was only done for smolts where final destinations could be determined ($N = 73$). Variance inflation factors (calculated using the R within the vif library) of flow properties and smolt characteristics were <3, indicating that multicollinearity was not severe. The model was then simplified using a stepwise approach.

Swimming speed and angular difference, as functions of the hydrodynamics for both the main water course and intake area (2D and 3D-data, respectively) were assessed by fitting multiple candidate models. Predictors considered were flow velocity components (u, v and w), turbulent kinetic energy and fish length. Models exploring swimming speed also included interactions between velocity components and angular difference between flow direction and smolt ground direction, while models exploring angular difference included interactions with swimming speed and the velocity components. The individual fish was always used as a random intercept, and temporal autocorrelation between data points was modelled with a first order autoregressive structure. Models considering swimming speed were fitted as multiple linear mixed effect models (LMM) utilizing the lme function within the nlme-library (Pinheiro et al., 2017). Models considering angular difference were fitted as generalized linear mixed effect models (GLMM), specifically as a variable dispersion beta regression model utilizing the glmmTMB-library (Brooks et al. 2017) which uses the parameterization in Ferrari and Cribari-Neto (2004). The angular difference for each data point was bound between 0 (exactly following the current, representing an angular difference of 0°) and 1 (swimming exactly counter current, representing an angular difference of 180°) following ($AngDif_i$-$AngDif_{min}$)/($AngDif_{max}$ - $AngDif_{min}$), where $AngDif_{min}$ = 0 and $AngDif_{max}$ = 180. Denoted, the AngDif-models can be expressed as:

$AngDif_{ij} \sim beta(\mu_{ij}\phi_{ij}, (1-\mu_{ij})\phi_{ij})$.

$E(AngDif_{ij}) = \mu_{ij}$.

$var.(AngDif_{ij}) = (\mu_{ij(1-}\mu_{ij}))/(1+\phi_{ij})$.

$logit(\mu_{ij}) = \sum_{k=1}^{p} \chi_{ijk}\beta_k + \varepsilon_{ij}$.

$log(\phi_{ij}) = \sum_{k=1}^{q} z_{ijk}\Upsilon_k$.

$\varepsilon_{ij} = \phi_{ij}\,\varepsilon_{ij-1} + individual_j$

$individual_j \sim N(0, \sigma^2_{individual})$

The expected values of AngDif observation i from individual j ($E(AngDif_{ij})$) is μ and was modelled via a logit link by a predictor function, and ϕ is the dispersion parameter and was modelled via a log link by a second predictor function. Here, $\beta = (\beta_1, \ldots, \beta_p)^T$ and $\Upsilon = (\Upsilon_1, \ldots, \Upsilon_q)^T$ are, respectively, px1 and qx1 vectors of unknown regression parameters, $\chi_i^T = (\chi_{i1}, \ldots, \chi_{ip}) \in \mathbb{R}^p$ and $z_i^T = (z_{i1}, \ldots, z_{iq}) \in \mathbb{R}^q$ are the explanatory variables of interest ($k + q < n$) which can either be similar or different sets of covariates. The models also included a random intercept (individual) with mean zero and variance $\sigma^2_{individual}$. An autoregressive process of order one ($\varepsilon_{ij} = \phi_{ij}\,\varepsilon_{ij-1} + individual_j$) was also included to

represent the dependency of one value of AngDif on the past value of AngDif for each individual fish. An information theoretic approach was performed using Akaike's information criterion (Akaike 1974; Burnham and Anderson 2002) to compare model fits objectively, and determine which was the most appropriate. AIC values and differences in AIC values (ΔAIC) between the candidate models were calculated utilizing the bbmle-library (Bolker and R Development Core Team 2017), and models which had ΔAIC > 2 were interpreted as having substantial support over the candidate models. For the LMM's, we model averaged all candidate models within ΔAIC < 2 utilizing the model.avg. function in the MuMIn-library (Bartoń 2016). For the beta distribution models exploring angular difference, the model selection was done in two steps. First, the most supported fixed effect structure was determined under a constant φ, and next the most supported dispersion model was decided for the best outcome from step one. We only considered additive effects in the dispersion model (parameter estimates for the most supported dispersion model can be seen in Supplementary Table 1, Appendix A). Validation of the linear effect models was made by examining histograms of the normalized residuals and plotting the normalized residuals against fitted values. Marginal and conditional R^2 for the linear effect models were calculated utilizing the MuMIn-library (Bartoń 2016). The GLMMs were validated utilizing the DHARMAa-library (Hartig 2018). We also tested the performance and generality of the GLMMs by parameterizing the models on a random draw of 70% of the individual smolts, and then compared the predicted values against observed values for the remaining 30% of the smolts. This process was repeated 100 times to get an average measure of the linear correlation between the predicted vs the observed (i.e. R^2), while taking the sensitivity of the sample into account.

3. Results

3.1. Validation of simulated hydraulics

The hydraulic model was found to reproduce well the flow field in the study area. Simulated hydraulic parameters were compared to measured data from an acoustic doppler current profiler (ADCP) to validate the SSIMM CFD model. Predicted flows followed the north-south orientation of the main watercourse throughout most of the domain, whereas flows were directed across the river channel towards the turbine entrance in closer proximity to the turbine entrance, consistent with the modelled extraction of water. Predicted flow directions were similar to those measured (circular correlation test, $t = 20.08$, $p < .001$, $r = 0.624$), with directions in both cases tending to be towards the south-south-east. Predicted resultant flow velocity increased with measured resultant flow velocity (Pearson's correlation test, $t = 23.75$, $p < .001$, $r = 0.489$), but there was a bias to the hydrodynamic model overestimating velocities at low measured velocities and underestimating velocities at high measured velocities.

3.2. Hydrodynamics

Hydrodynamics of the flow in the main water course and in the intake area varied with total flow discharge (Q) and percentage of flow going through the turbines (PerQ) (Fig. 1). The percentage of flow going through the turbines was the main determinant of variation in flow pattern, flow velocities and turbulence kinetic energy (TKE) in the horizontal (uv), transversal vertical (vw) and longitudinal vertical planes (uw) (Supplementary Table 2, Appendix A).

The main water course was characterised by a flow pattern with low water velocities at the right bank of the river (opposite to the intake) which changed orientation towards the intake area with a concomitant increase of water velocity and TKE (Fig. 1). This change occurred closer to the bank under higher Q (Fig. 1) with velocities and TKE increasing with PerQ (Supplementary Table 2, Appendix A). TKE and mean velocities in the longitudinal vertical plane peaked in the intake area with the highest values occurring from the surface down to middle water column depths (approximately 1 to 2 m below the wall at the intake) (Supplementary Table 3, Appendix A). The intake area was also characterised by strong variations on the vertical velocities which increased with PerQ peaking at the middle of the water column towards the bottom (Supplementary Table 3, Appendix A) as result of the presence of a 2 m vertical wall in front of the submerged HP intake. The intake area exhibited strong recirculation areas extending through the entire water column.

3.3. Fish migratory movement

Fish behaviour and migration route varied greatly among individuals. Among the 76 fish detected by the receiver array, 32 migrated to the turbine intake (mainly directly, $N = 25$), 41 moved to the downstream weir showing more meandering behaviour, and three moved around in the study area for prolonged periods and their final route selection was not detected. Migration route (into the turbine or to the downstream weir) depended on the initial location of the fish in the system and PerQ (Table 1). More fish entered the turbine under high PerQ. Moreover, fish entering on the right bank (away from the turbine intake), where the velocities were lower and the flow mainly moved towards the weir, were more likely to migrate downstream (81.9%) than those entering on the left bank (34.8%), where the main flow went towards the turbine intake (Fig. 2). These results support the assumption that smolts do to some extent follow the main flow.

Fine scale behaviour responses to flow kinematics, as quantified by angular difference and swimming speed (see details in Material and Methods), however, showed that the smolts did not strictly follow the flow. The most supported models connected fish divergence from flow directions and swimming speed with TKE, the three components of velocity and with the interaction between the two (Tables 2 and 3, Figs. 3, 4 5 and 6). For both the main water course and the intake area the developed models explained a considerable proportion of the variation in swimming speeds (marginal $R^2 = 32\%$ and 38%, respectively, Table 3) and swimming direction relative to the flow (hold-out-sample $R^2_{70\%} = 40\%$ and 26%, respectively).

Fish swimming speed and swimming direction were interconnected, and their variation could be linked to the different swimming capacity modes as quantified from Booth et al. (1997) (Fig. 7). Fish swam at low speeds below their sustained swimming speed (0.38 m s^{-1}) when swimming in a similar direction to the flow, at higher prolonged swimming speeds (0.38–0.73 m s^{-1}) when moving away from the flow (Fig. 3b,d, 4b,d, and 5e,f), and could even exceed their estimated burst swimming speed (> 0.73 m s^{-1}) when moving in the opposite direction of the flow in the intake area (Fig. 4b,d). Rapid swimming was more prominent in the intake area where higher variation (magnitude and direction) of vertical and longitudinal velocities and the highest TKE occurred (Fig. 4). In the intake area, fish moved away from the flow by swimming at speeds >0.38 m s^{-1} (within fish prolonged swimming speed) in areas with lower downward vertical velocities or higher upstream velocities (Table 2, Fig. 4b, d). This was mainly evident in areas where the resultant longitudinal vertical velocities did not exceed the sustained swimming capacity of fish (Fig. 7, Fig. 4e and Fig. 6d).

Table 1
Probability of a smolt migrating downstream as opposed to entering the turbine as a function of discharge (Q), proportion of flow entering the turbine (PerQ), and location where first detected (InLoc).

	Estimate	Std. error	z value	Pr(>|z|)
(Intercept)	38.351	16.692	2.297	0.022
Discharge (Q)	−0.319	0.159	−2.003	0.045
PerQ	−0.108	0.029	−3.720	<0.001
InLoc(Central right)	−0.691	1.091	−0.633	0.527
InLoc(Central left)	−1.658	1.177	−1.408	0.159
InLoc(Left bank)	−2.755	1.120	−2.459	0.014

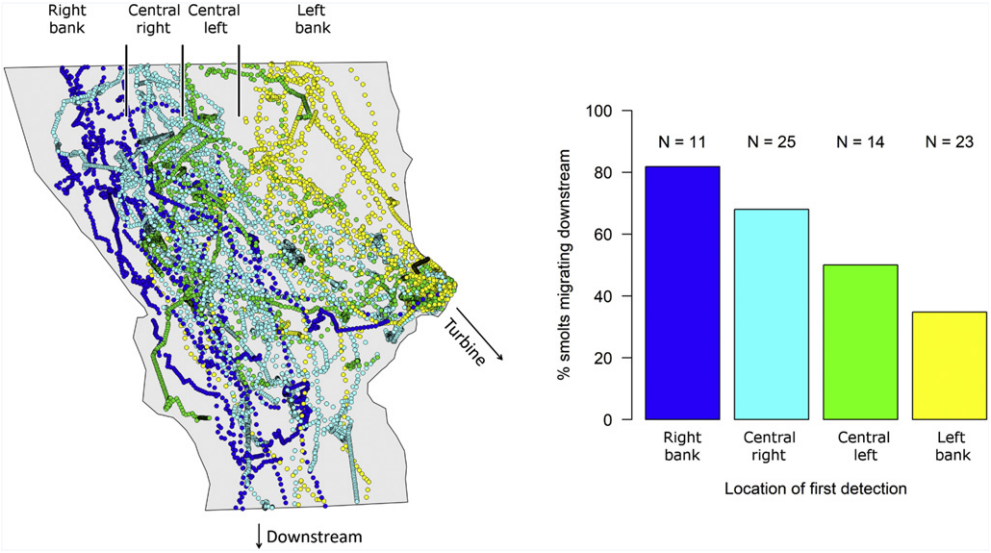

Fig. 2. Estimated positions of fish (left panel) and migration destination according to location of first detection (right panel).

In the intake area TKE peaked (max = 0.24 $m^2 s^{-2}$, Table 2, Supplementary Tables 2 and 3, Appendix A) and fish moved at very different directions from the flow (Fig. 4a). Here, burst swimming speeds (> 0.73 m s^{-1}) were used by the fish to swim in areas with very high TKE associated with high downstream and high downward vertical velocities (Table 3, Fig. 6a, b). The effect of TKE on fish swimming speed was conditioned by the direction of the flow (Fig. 4a). For the same conditions of high TKE, fish diverged from the flow by swimming slower in areas with high upstream and low downward velocities (Fig. 6a, b). Overall, upstream velocities in the intake area always reduced fish swimming speed (Table 3, Fig. 6c).

In the main water course, where the flow mainly moved in the downstream direction, variation in vertical velocity was negligible and TKE was lower (max = 0.03 $m^2 s^{-2}$) than in the intake area. Areas of low downstream velocities and low TKE allowed for fish to swim slower (< 0.30 m s^{-1}) and to still be able to deviate from the flow direction (Table 2, Fig. 3a, 5a). The effects of TKE on swimming speed outweighed the effects of the transversal velocities in this area, as fish always swam faster at the highest TKE independent of the transversal velocities (Fig. 5b). Both, fish swimming speed and divergence from the flow were found to be restricted by high downstream velocities combined with high transversal velocities, when resultant velocities were higher than 0.5 m s^{-1}, above the fish sustained swimming speed (Table 2, Fig. 7, Fig. 3c, Fig. 5c).

Table 2
Statistical outputs from the generalized linear mixed effect models (with beta-distributions) for angular difference in the main water course (2D-domain) and intake area (3D-domain). Both models used the individual fish as a random effect. Parameter estimates are presented for the fixed effects only, with the standard error in parentheses. R^2_{All} is calculated by comparing observed values vs predicted values for the model, and $R^2_{70\%}$ is calculated by parameterising the model on 70% of the individuals and compare the observed vs predicted for the remaining 30% of the individuals. This process was repeated 100 times assess the generality of the model. The value for $R^2_{70\%}$ represents the mean of the 100 repetitions, and the SD from this process is shown in parentheses.

	Dependent variables:	
	Angular difference	Angular difference
	(main water course)	(intake area)
Intercept	−3.59*** (0.22)	−3.39*** (0.35)
v	−9.48*** (0.74)	−10.48*** (0.90)
TKE	391.75*** (103.66)	49.38** (16.69)
u	7.41*** (0.78)	−1.94 (1.48)
Swimming speed	25.63*** (0.51)	16.63*** (0.55)
Swimming speed x TKE	−5486.81*** (190.10)	–
Swimming speed x u	21.48*** (1.25)	20.31*** (2.56)
TKE x u	−3194.79*** (384.44)	308.68** (94.46)
u x v	−18.04*** (2.58)	−19.85*** (4.00)
w	–	−14.15*** (2.45)
Swimming speed x w	–	48.26*** (5.97)
u x w	–	−1.18*** (0.35)
Observations	12,072	1971
R^2_{All}	0.84	0.86
$R^2_{70\%}$	0.40 (0.08)	0.26 (0.15)

** Significant in P < 0.01.
*** Significant in P < 0.001.

Table 3
Statistical outputs from the most supported linear mixed effects models for swimming speed in the main water course (2D-domain) and intake area (3D-domain). Both models included the individual fish as a random effect. Parameter estimates are presented for the fixed effects only, with the standard error in parentheses. The parameter estimates are a result of averaging over all models within ΔAIC < 2 for the respective set of candidate models.

	Dependent variables:	
	Swimming speed	Swimming speed
	(main water course)	(intake area)
Intercept	−0.08 (0.10)	0.20** (0.08)
v	0.67*** (0.07)	0.43*** (0.07)
TKE	21.51** (8.17)	−12.32*** (2.62)
u	−0.78*** (0.05)	0.02 (0.08)
w	−8.06 (5.02)	0.01 (0.17)
Len	0.01 (0.01)	−0.01 (0.01)
Angular Difference	0.09*** (0.01)	−0.06* (0.03)
Angular Difference x v	−0.35*** (0.04)	0.55*** (0.08)
Angular Difference x u	−0.01 (0.02)	−0.21*** (0.05)
Angular Difference x TKE	125.60*** (4.94)	11.48*** (2.27)
TKE x u	143.90*** (30.70)	−49.28*** (6.04)
TKE x w	−2715 (1866)	−70.36*** (13.58)
u x v	0.85*** (0.19)	0.59* (0.24)
u x w	−28.83* (12.31)	−1.19*** (0.35)
TKE x v	−62.54* (29.45)	4.36 (5.40)
v x w	0.83 (5.85)	−0.33 (0.51)
Observations	12,072	1971
Marginal R^2	0.32	0.38
Conditional R^2	0.60	0.81

* Significant in P < 0.05.
** Significant in P < 0.01.
*** Significant in P < 0.001.

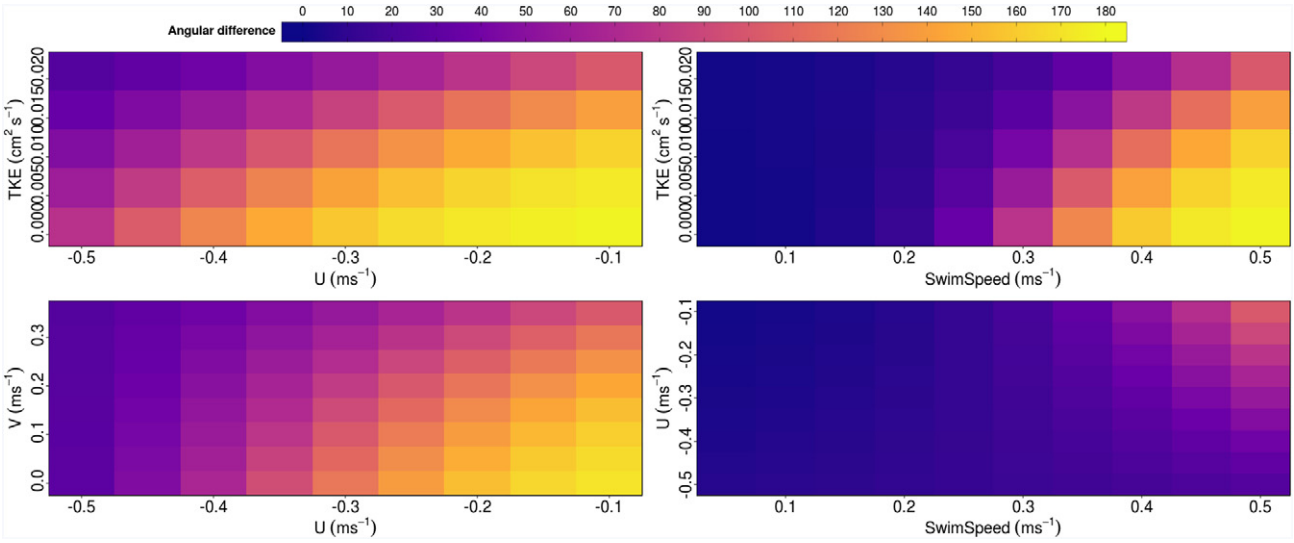

Fig. 3. Heatmap plot showing the effect of the interactions among TKE, u, v, and swimming speed on the variation of the estimated angular difference (0 = with the current and 180 = against the current) in the main water course.

4. Discussion

In the present study a biophysical-biomechanical perspective was taken, in which fish movement is considered to result from the interplay between fish and the hydrodynamics of the flow (surrounding). However, we acknowledge the importance of endogenous factors (e.g. motivation and physical condition) mediating behavioural and movement of fish and the possibility that the behavioural responses of fish could have been partially conditioned by the proximity to the intake and that fish could have exhibited a different behaviour if facing a different type of hydraulic structure (e.g weir, spillways). The large-scale spatial distribution and fate of fish was found to be related to fish starting location in the study area and to the main flow, in particular with PerQ. These results indicated that to some extent fish do follow the main flow as postulated by several authors (Rivinoja 2005; Williams et al., 2012). Interestingly, the fish also moved downwards flow towards the submerged intake (2 m), a behaviour with no natural parallel in rivers. However, our analyses showed that fish fine-scale decisions results from the interplay with fine-scale multi interactive hydraulic cues. These cues are critical factors that affect the technical execution of directional changes as well as swimming speed, determining the course of the journey. Fine-scale temporal and spatial variation in the field motion may be detected by the mechanosensory system of fish (Oteiza et al., 2017) and induce different behavioural responses such as variation in rheotaxic response, fatigue, and disorientation (Enders et al. 2012; Jonsson and Ruud-Hansen 1985).

Fish three-dimensional swimming direction and speed depended on the interplay among TKE and the three-dimensional components of water velocity and the interaction between the two and could be linked to fish swimming modes. Fish swam in similar direction to the flow at

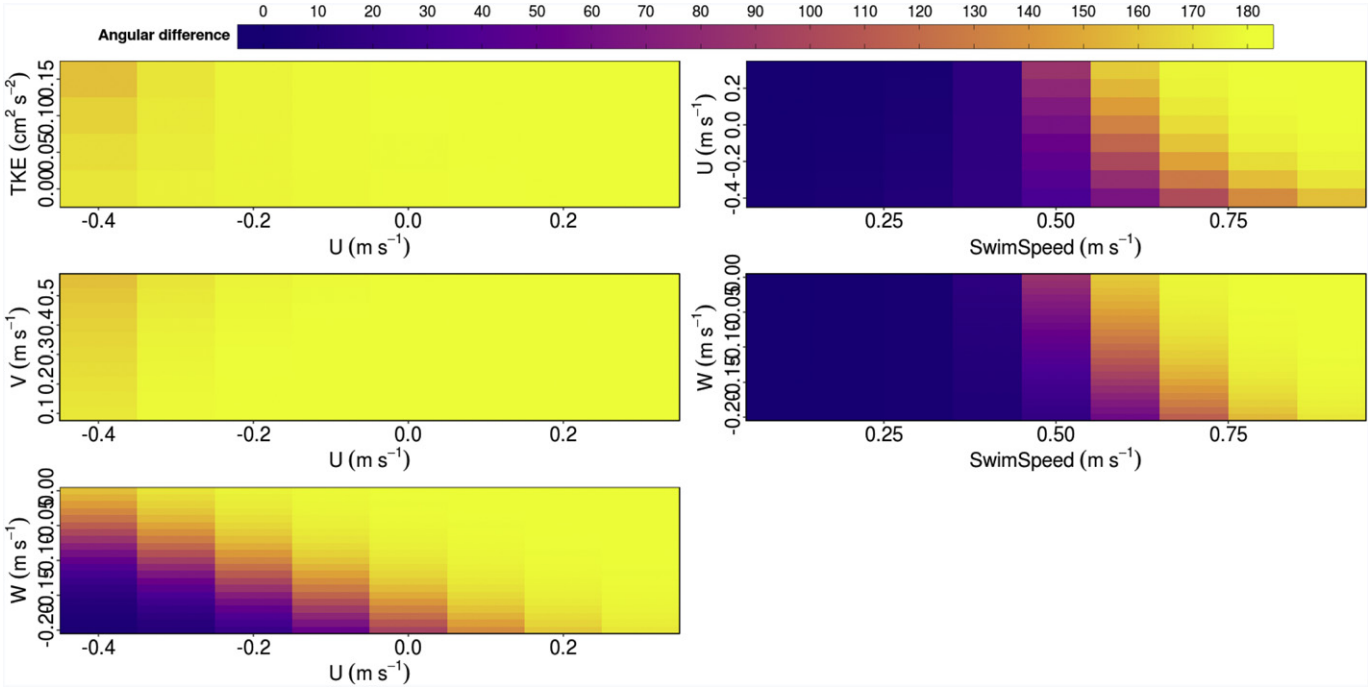

Fig. 4. Heatmap plot showing the effect of the interactions among TKE, u, v, w and swimming speed on the variation of the estimated angular difference (0 = with the current and 180 = against the current) in the intake area.

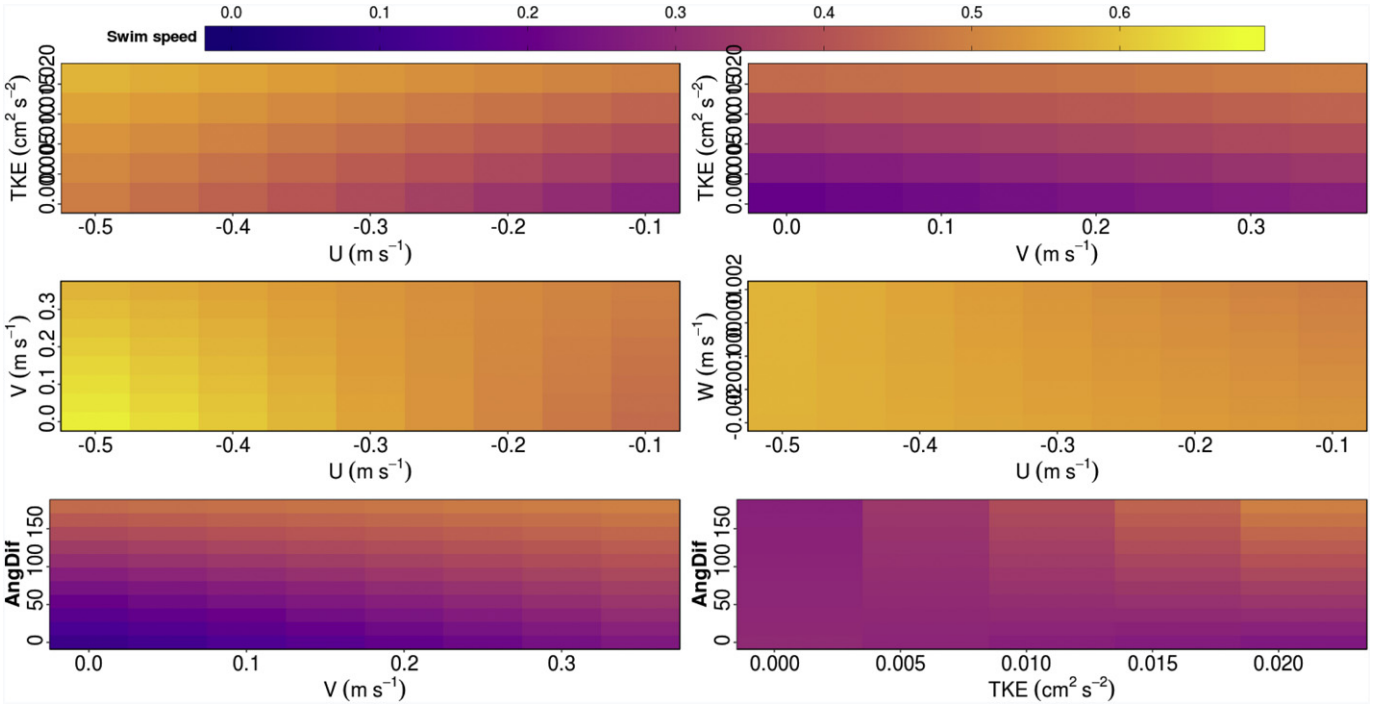

Fig. 5. Heatmap plot showing the effect of the interactions among TKE, u, v, w and angular difference (AngDif) on the variation of the estimated swimming speed in the main water course.

swimming speeds below their sustained swimming capacity (0.38 m s^{-1}), diverged from the flow by swimming at higher prolonged swimming speeds (0.38–0.73 m s^{-1}) and swam in the opposite direction to the flow at speeds that exceeded their estimated burst swimming speed (> 0.73 m s^{-1}). The transition among such behaviours depended on the hydrodynamic context. In the intake area where the highest three-dimensional velocities and TKE occurred, fish always swam fast, generally above their prolonged swimming speed, and in different directions, indicating that fish were actively swimming and trying to escape the unsuitable turbulent conditions. Fish tend to avoid unpredictable flows with wide fluctuations in velocities, flow features that both at spatial and temporal scales can interfere with their swimming performance (Enders et al. 2003; Smith, 2003). Interestingly, for the same magnitude of TKE, depending on the direction of the longitudinal velocities, fish swam at different direction from the flow by using different swimming speeds. Fish diverged from the flow swimming slower or at similar speeds than the longitudinal velocities when swimming under higher upstream velocities. This shows that fish were either drifting or actively swimming against the flow to escape such conditions. Previous studies have shown that high turbulence increase cost of locomotion (Liao et al. 2003; Odeh et al., 2002). It is thus likely that the high upstream velocities and high TKE associated to the strong recirculation in the intake area have increased energetic costs associated with fish swimming performance and station holding

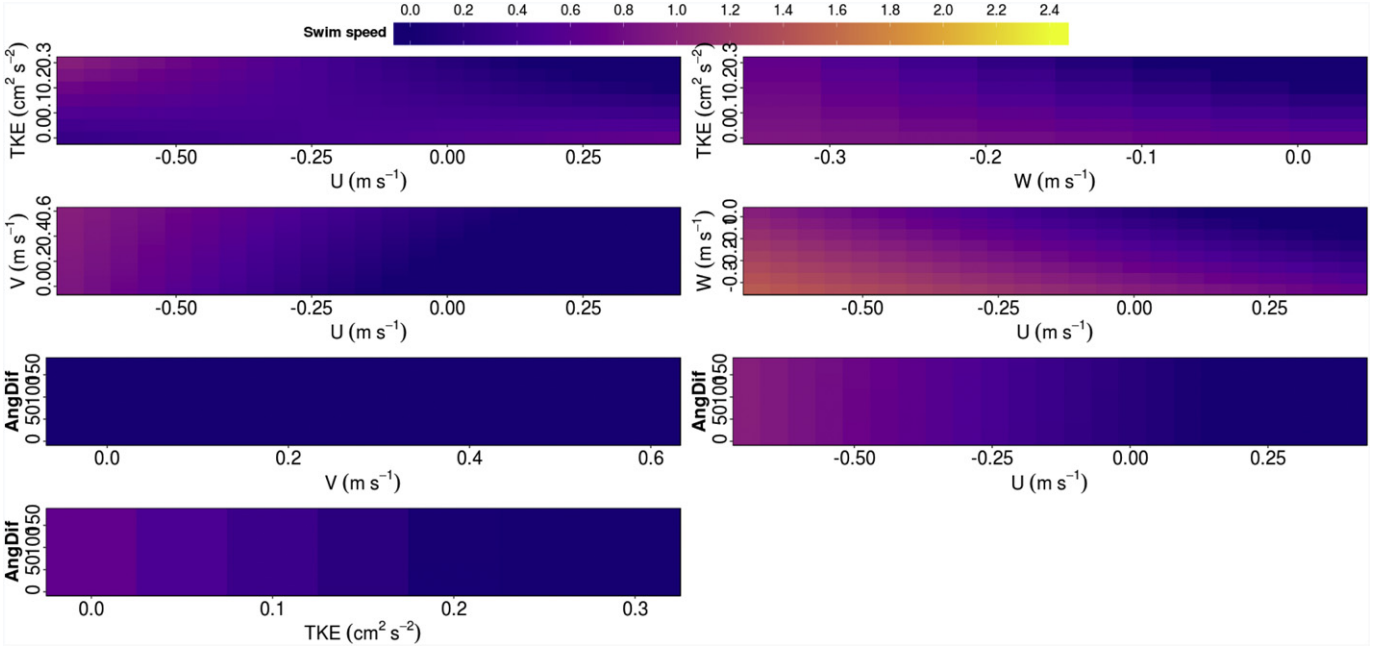

Fig. 6. Heatmap plot showing the effect of the interactions among TKE, u, v, w and angular difference (AngDif) on the variation of the estimated swimming speed in the intake area.

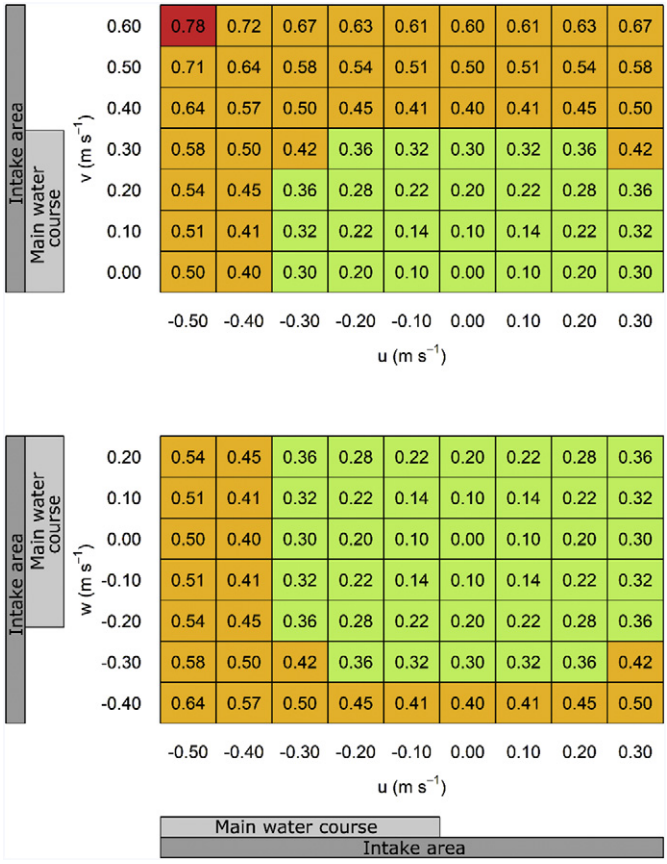

Fig. 7. The resultant velocities (numbers in cells) of the flow for the horizontal (V_{uv}, upper panel) and longitudinal vertical planes (V_{uw}, lower panel) classified according to swimming modes (estimated from Booth et al. 1997, considering temperatures and smolt size): sustained swimming speed (<0.38 m s^{-1}) in green, prolonged swimming speed (0.38–0.73 m s^{-1}) in orange, and burst swimming speed (>0.73 m s^{-1}) in red. The bars indicate the range in velocity components found in the main water course and the intake area.

(Enders et al. 2005; Pavlov et al. 1982; Silva et al. 2011). Contrarily in the main water course the relative low values of TKE seemed to have allowed for fish to keep their stability and swimming capacity. Several laboratory studies have shown that steady predictable flows, similar to the flow in the main water course, can be exploited by fish for propulsion (Hinch and Rand 2000; Liao et al. 2003; Montgomery et al. 2003; Smith et al., 2003). In the main water course under low TKE associated with low longitudinal velocities, fish could diverge from the flow without swimming very fast (close to their sustained swimming speed). In contrast, under higher TKE and higher longitudinal velocities, the fish had to swim faster to diverge from the flow. This variation of fish behaviour in response to turbulence levels shows that the magnitude of turbulence plays an important role in determining fish behaviour.

Our results indicate that the magnitude of TKE in the main water course (TKE < 0.03 m^2 s^{-2}) are suitable for fish navigation and stabilization in contrast to the high levels of TKE in the intake area (0.03 < TKE < 0.24 m^2 s^{-2}) which hamper fish swimming performance. Our findings support the theory of a two-fold effects of turbulence on fish swimming performance (Liao 2007; Odeh et al., 2002) which postulates that fish can experience disorientation and displacement when swimming under high turbulence associated with large recirculation areas, such as those found in the intake area. Moreover, under lower turbulence fish can reduce locomotory costs and enhance performance by capturing the energy of discrete vortices of a diameter smaller than their length (below 2/3 of fish total length) (Przybilla et al., 2010; Silva et al. 2012), likely present in the main water course. Depending on the turbulence levels, turbulence might then be considered both a beneficial or constraining hydrodynamic feature for fish swimming performance. The upper limit of turbulence of the hydrodynamic and fish behaviour interaction should then be set by the destabilization 'threshold' of a swimming fish.

Although the magnitude of the hydraulic variables was shown to play an important role in determining fish swimming speed and fish swimming direction, the direction of the flow was found to be more important in determining such behaviours. Therefore, the interaction of two hydraulic variables with the same magnitude can induce different behavioural responses depending on the direction of the flow. Our findings support that fish adopt different responses based on a bioenergetic strategy to cope with the continuous compensation for displacement by the heterogeneity of the flow (Chapman et al. 2011). The strategy of moving with the flow, the most favourable for movement, is a well know strategy adopted by animals (Chapman et al. 2011). The strategy adopted by fish to cope with the increment of vertical velocities towards the bottom also supports a bioenergetic strategy used during swimming. Fish are not equally sensitive to disturbances in all planes, and the direction of the perturbation relative to the body plays a critical role in determining fish response (Webb 2004). By swimming fast when the vertical longitudinal velocities were very high, related to unstable and irregular pitching motions, fish may decrease their energetic cost associated with correcting for pitching and restoring balance and stabilization. Correcting for variation in vertical forces of the flow are generally regarded as more energetically demanding than correcting for disturbances from other directions, because it requires the production of vertical forces, either anterior or posterior to the centre of mass (Liao 2007).

In our study, high resolution telemetry and 3D hydraulic modelling contributed to the understanding of fish fine-scale behaviour in terms of swimming speed and swimming direction, which were found to depend on the interplay between fish and the interaction of multiple hydraulic variables. The results illustrates the importance of considering and accessing the interaction of multiple hydraulic variables acting together when analysing the effects of hydraulics on fish swimming performance, in contrast to what has been the typical approach in the literature. We found that flow direction impacted fish behaviour and swimming performance more than the magnitude of flow velocity. This is important, because design solutions for fish passage have primarily been based on the thresholds of flow velocity and turbulence magnitudes that have been considered suitable for fish swimming. The statistical explanatory models of this study may then be developed into quantitative prediction tools that can support and inform decision making in future management and engineering solutions for safe fish migration past barriers. While our models successfully explained swimming speed and swimming direction responses, they remain to be validated in other systems.

Declaration of competing interest

The authors declare no competing interest

Acknowledgements

This research was supported by the SafePass project (Project no. 244022) funded by the Research Council of Norway (RCN) under the ENERGIX program,13 hydropower companies, the Norwegian Environment Agency and the Norwegian Water Resources and Energy Directorate. Additional funding was provided by the Norwegian Research Centre for Hydropower Technology – HydroCen (Project no. 257588). We would like to thank to Dr. Jeffrey A. Tuhtan from the Environmental Sensing and Intelligence, Centre for Biorobotics of Tallinn University of Technology for useful suggestions. We also thank Ingebrigt Uglem from NINA for assisting during tagging of the fish.

Authors contributions

A.T.S., K.Ø.G., F.Ø., H.B. and T.F. conceived the ideas and designed methodology; A.T.S., H.P.F., K.Ø.G., F.Ø., and H.B. collected the data; A.T.S., R.D.H., K.M.B. and H.B. analysed the data; A.T.S. led the writing of the manuscript. All authors contributed critically to the drafts and gave final approval for publication

Appendix A. Supplementary data

Supplementary data to this article can be found online at https://doi.org/10.1016/j.scitotenv.2019.135773.

References

R Core Team. R, 2017. A Language and Environment for Statistical Computing. R Foundation for Statistical Computing, Vienna, Austrintake area.

Akaike, H., 1974. A new look at the statistical model identification. IEEE Trans. Autom. Control 19, 716–723.

Baktoft, H., Gjelland, K.Ø., Økland, F., Thygesen, U.H., 2017. Positioning of aquatic animals based on time-of-arrival and random walk models using YAPS (Yet Another Positioning Solver). Sci. Rep. 7, 14294.

Bartoń, K., 2016. MuMIn: Multi-Model Inference (R package version 1.15.6).

Bleckmann, H., Zelick, R., 2009. Lateral line system of fish. Integr Zool 4, 13–15.

Bolker, B., R Development Core Team, 2017. bbmle: Tools for General Maximum Likelihood Estimation. R Package Version 1.0.20. https://CRAN.R-project.org/package=bbmle.

Booth, R.K., Bombardier, E.B., McKinley, R.S., Scruton, D.A., Goosney, R.F., 1997. Swimming performance of post spawning adult (kelts) and juvenile (smolts) Atlantic salmon, *Salmo salar*. Can. Manuscr. Rep. Fish. Aquat. Sci. 2406 (V + 18).

Brönmark, C., Hulthén, K., Nilsson, P.A., Skov, C., Hansson, L.A., Brodersen, J., et al., 2013. There and back again: migration in freshwater fishes. Can. J. Zool. 92, 467–479 (There and back again: migration in freshwater fishes. Can. J. Zool. 92(6), 467-479).

Brooks, M.E., Kristensen, K., van Benthem, K.J., Magnusson, A., Berg, C.W., Nielsen, A., Skaug, H.J., Maechler Bolker, B.M., 2017. glmmTMB balances speed and flexibility among packages for zero-inflated generalized linear mixed modeling. The R Journal 9 (2), 378–400 https://journal.r-project.org/archive/2017/RJ-2017-066/index.html.

Burnham, K.P., Anderson, D.R., 2002. Model Selection and Multimodel Inference. Springer Science, Business Media.

Chapman, J.W., Klaassen, R.H.G., Drake, V.A., Fossette, S., Hays, G.C., Metcalfe, J.D., Reynolds, A.M., Reynolds, D.R., Alerstam, T., 2011. Animal orientation strategies for movement in flows. Curr. Biol. 21, R861–R870.

Chen, S.H., 2006. Finite Difference Method. High-Field Physics and Ultrafast Technology Laboratory, Taipei, Tawan.

Cotel, A.J., Webb, P.W., Tritico, H., 2006. Do brown trout choose locations with reduce turbulence? Trans. Am. Fish. Soc. 135, 610–619.

Coutant, C.C., 2001. Integrated, multi-sensory, behavioral guidance systems for fish diversions. In: Coutant, C.C. (Ed.), Behavioral Technologies for Fish Guidance. 26. American Fisheries Society, Symposium, Bethesda, MD, pp. 105–113.

Enders, E.C., Boisclair, D., Roy, A.G., 2003. The effect of turbulence on the cost of swimming for juvenile Atlantic salmon (Salmo salar). Can. J. Fish. Aquat. Sci. 60, 1149–1160.

Enders, E.C., Boisclair, D., Roy, A.G., 2005. A model of the total swimming costs in turbulent flow for Atlantic salmon (*Salmo salar*). Can. J. Fish. Aquat. Sci. 62, 1079–1089.

Enders, E.C., Gessel, M.H., Anderson, J.J., Williams, J.G., 2012. Effects of decelerating and accelerating flows on juvenile salmonid behavior. Trans. Am. Fish. Soc. 141 (2), 357–364.

Ferrari, S.L.P., Cribari-Neto, F., 2004. Beta regression for modelling rates and proportions. J. Appl. Stat. 31 (7), 799–815.

Fjeldstad, H.P., Uglem, I., Diserud, O.H., Fiske, P., Forseth, T., Kvingedal, E., et al., 2012. A concept for improving Atlantic salmon Salmo salar smolt migration past hydro power intakes. J. Fish Biol. 81, 642–663.

Goodwin, A., Politano, M.S., Garvin, J.W., Nestler, J., Hay, D., Anderson, J.J., et al., 2014. Fish navigation of large dams emerges from their modulation of flow field experience. Proc. Natl. Acad. Sci. U. S. A. 111, 5277–5282.

Hartig, F., 2018. DHARMa: Residual Diagnostics for Hierarchical (MultiLevel/Mixed) Regression Models. R Package Version 0.2.0.

Hinch, S.G., Rand, P.S., 2000. Optimal swimming speeds and forward-assisted propulsion: energy-conserving behaviours of upriver-migrating adult salmon. Can. J. Fish. Aquat. Sci. 57, 2470–2478.

Hugh Dingle, V., Drake, A., 2007. What is migration? Bioscience 57 (2), 1 113–121.

Jonsson, B., Ruud-Hansen, J., 1985. Water temperature as the primary influence on timing of seaward migrations of Atlantic salmon (*Salmo salar*) smolts. Can. J. Fish. Aquat. Sci. 42, 593–595.

Liao, J.C., 2007. A review of fish swimming mechanics and behavior in altered flows. Phil. Trans. R. Soc. B 362, 1973–1993.

Liao, J.C., Beal, D.N., Lauder, G.V., Triantafyllou, M.S., 2003. The Ka'rma'n gait: novel kinematics of rainbow trout swimming in a vortex street. J. Exp. Biol. 206, 1059–1073.

Lucas, M.C., Baras, E., 2001. Migration of Freshwater Fishes. Blackwell Science, Oxford, UK.

Lupandin, A.I., 2005. Effect of flow turbulence on swimming speed of fish. Biol. Bull. 32, 461–466.

Montgomery, J., Baker, C., Carton, A., 1997. The lateral line can mediate rheotaxis in fish. Nature 389, 960–963.

Montgomery, J.C., McDonald, F., Baker, C.F., Carton, A.G., Ling, N., 2003. Sensory integration in the hydrodynamic world of rainbow trout. Proc. R. Soc. B 270, S195–S197.

Nilsson, C., Reidy, C.A., Dynesius, M., Revenga, C., 2005. Fragmentation and flow regulation of the world's large river systems. Science 308, 405–408.

Odeh, M., Noreika, J.F., Haro, A., Maynard, A., Castro-Santos, T., Cada, G.F., 2002. Evaluation of the effects of turbulence on the behavior of migratory fish. Final Report 2002, Report to Bonneville Power Administration, Contract No. 00000022, pp. 1–55.

Olsen, N.R.B., 2009. A three-dimensional numerical model for simulation of sediment movements in water intakes with multi-block option. User's Manual. Department of Hydraulic and Environmental Engineering, The Norwegian University of Science and Technology, Trondheim, Norway.

Oteiza, P., Odstrcil, I., Lauder, G., Portugues, R., Engert, F., 2017. A novel mechanism for mechanosensory-based rheotaxis in larval zebrafish. Nature 547, 445–448.

Pavlov, D.S., Skorobagatov, M.A., Shtaf, L.G., 1982. The critical current velocity of fish and the degree of flow turbulence. Rep. USSR Acad. Sci. 267, 1019–1021.

Pinheiro, J., Bates, D., DebRoy, S., Sarkar, D., R Core Team, 2017. nlme: Linear and Nonlinear Mixed Effects Models. R Package Version 3.1-131. https://CRAN.R-project.org/package=nlme.

Poff, N.L., Allan, J.D., Bain, M.B., Karr, J.R., Prestegaard, K.L., Richter, B.D., Sparks, R.E., Stromberg, J.C., 1997. The natural flow regime: a paradigm for river conservation and restoration. BioScience 47, 769–784.

Przybilla, A., Kunze, S., Rudert, A., Bleckmann, H., Brucker, C., 2010. Entraining in trout: a behavioural and hydrodynamic analysis. J. Exp. Biol. 213, 2976–2986.

Rivinoja, P., 2005. Migration Problems of Atlantic Salmon (*Salmo salar* L.) in Flow Regulated Rivers. Doctoral thesis 2005: 114. ISSN: 1652-6880. ISBN: 91-576-6913-9. Department of Aquaculture, Swedish University of Agricultural Science, Umeå, Sweden.

Silva, A.T., Santos, J.M., Ferreira, M.T., Pinheiro, A.N., Katopodis, C., 2011. Effects of water velocity and turbulence on the behaviour of Iberian barbell (*Luciobarbus bocagei*, Steindachner 1864) in an experimental pool-type fishway. River Res. Appl. 27, 360–373.

Silva, A.T., Katopodis, C., Santos, J.M., Ferreira, M.T., Pinheiro, A.N., 2012. Cyprinid swimming behaviour in response to turbulent flow. Ecol. Eng. 44, 314–328.

Silva, A.T., Lucas, M.C., Castro-Santos, T., Katopodis, C., Baumgartner, L.J., Thiem, J.D., Aarestrup, K., Pompeu, P., O'Brien, G.C., Braun, D., Burnett, N.J., Zhu, D.Z., Fjeldstad, H.P., Forseth, T., Rajaratnam, N., Williams, J.G., Cooke, S., 2018. The future of fish passage science, engineering, and practice. Fish Fish. 19, 340–362.

Smith, D.L., 2003. The Shear Flow Environment of Juvenile Salmonids. PhD thesis. University of Idaho.

Thorstad, E.B., Whoriskey, F., Uglem, I., Moore, A., Rikardsen, A.H., Finstad, B.A., 2012. Critical life stage of the Atlantic salmon *Salmo salar*: behaviour and survival during the smolt and initial post-smolt migration. J. Fish Biol. 81, 500–542.

Voigt, R., Carton, A.G., Montgomery, J.C., 2000. Responses of anterior lateral line afferent neurons to water flow. J. Exp. Biol. 203, 2495–2502.

Webb, P.W., 2004. Response latencies to postural differences in three species of teleostean fishes. J. Exp. Biol. 207, 955–961.

Williams, J.G., Armstrong, G., Katopodis, C., Larinier, M., Travade, F., 2012. Thinking like a fish: a key ingredient for development of effective fish passage facilities at river obstructions. River Res. Appl. 28, 407–417.